NIH Public Access
Author Manuscript
Faraday Discuss. Author manuscript; available in PMC 2014 March 15.

Published in final edited form as:
Faraday Discuss. 2013 ; 166: 285–301.

Self-Assembly of Natural and Synthetic Drug Amphiphiles into Discrete Supramolecular Nanostructures

Lye Lin Lock[a], **Michelle LaComb**[b], **Kelly Schwarz**[a,c], **Andrew G. Cheetham**[a], **Yi-an Lin**[a], **Pengcheng Zhang**[a], and **Honggang Cui**[a]

Honggang Cui: hcui6@jhu.edu

[a]Department of Chemical and Biomolecular Engineering, and Institute of NanoBioTechnology, The Johns Hopkins University, 3400 North Charles Street, Baltimore MD 21218, United States, Fax: 410-516-5510; Tel:410-516-6878

[b]Department of Chemistry, Rice University, 6100 Main St. Houston, TX 77251, United States

Abstract

Molecular assembly provides an effective approach to construct discrete supramolecular nanostructures of various sizes and shapes in a simple manner. One important technological application of the resulting nanostructures is their potential use as anticancer drug carriers to facilitate targeted delivery to tumour sites and consequently to improve clinical outcomes. In this carrier-assisted delivery strategy, anticancer drugs have been almost exclusively considered as the cargo to be carried and delivered, and their potential as molecular building blocks has been largely ignored. In this discussion, we report the use of anticancer drugs as molecular building units to create discrete supramolecular nanostructures that contain a high and quantitative drug loading and also have the potential for self-delivery. We first show the direct assembly of two amphiphilic drug molecules (methotrexate and folic acid) into discrete nanostructures. Our results reveal that folic acid exhibits rich self-assembly behaviours *via* Hoogsteen hydrogen bonding in various solvent conditions, whereas methotrexate was unable to assemble into any well-defined nanostructures under the same conditions, despite its similar chemical structures. Considering the low water solubility of most anticancer drugs, hydrophilic segments must be conjugated to the drug in order to bestow the necessary amphiphilicity. We have demonstrated this for camptothecin through the attachment of β-sheet-forming peptides with overall hydrophilicity. We found that the intermolecular interactions among camptothecin segments and those among β-sheet peptides act together to define the formation of stable one-dimensional nanostructures in dilute solutions, giving rise to nanotubes or nanofibers depending upon the processing conditions used. These results lead us to believe that self-assembly of drugs into discrete nanostructures not only offers an innovative way to craft self-delivering anticancer drugs, but also extends the paradigm of using molecular assembly as a toolbox to achieve functional nanostructures, to a new area which is specifically focused on the direct assembly of functional molecules (e.g. drugs, or imaging agents) into nanostructures of their own.

Introduction

Drugs are a special class of chemicals that produce a biological effect when administered to a living organism. In clinical practice, drugs are often co-administered with other

© The Royal Society of Chemistry [year]

Correspondence to: Honggang Cui, hcui6@jhu.edu.

[c]Current address: Department of Chemical and Biological Engineering, Northwestern University, 2145 Sheridan Road Technological Institute E-136, Evanston, IL 60208, United States.

NIH-PA Author Manuscript
NIH-PA Author Manuscript
NIH-PA Author Manuscript

NIH-PA Author Manuscript

NIH-PA Author Manuscript

NIH-PA Author Manuscript

substances, such as excipients, stabilizers, solvents, or even other drugs, to maximize the therapeutic effects while minimizing the possible side effects. Given the low therapeutic index of most anticancer drugs (the ratio of the lethal or toxic dose to the therapeutic dose) and their great toxicity toward healthy cells, it is important and desirable to maintain a high therapeutic level of drugs only in the tumour sites.[1] Over the past three decades, the use of nanoscale carriers to modify the drug's pharmacokinetic properties and biodistribution profiles has been the primary focus of research in the drug delivery community, with the goal of achieving targeted delivery to tumour sites.[2–9] Two main strategies have been actively pursued: the first involves covalently modifying hydrophobic drugs with hydrophilic polymers to form polymer-drug conjugates.[2–4] The purpose of this conjugation is to improve drug solubility, to increase drug targeting efficiency and to reduce drug toxicity. The great advantage of this strategy is that the pharmacokinetic properties of the drug are determined by the molecular weight and characteristics of the conjugated polymers. However, this strategy is limited by the polydispersity in polymer length and drug loading per polymer chain, and also by the limited choice of hydrophilic polymer due to concerns regarding potential cytotoxicity and biodegradability.[2,3,10]

The other strategy is the use of well-defined nanoscale architectures, with drugs being either encapsulated within, or conjugated onto, the carriers.[6–9] These nanocarriers often present well-defined size, shape and tuneable surface chemistries, allowing robust pharmacokinetic protocols independent of the drug encapsulated to be established. A great diversity of nanostructures have been evaluated for their potential applications as drug carriers, including liposomes,[11] vesicles,[12] dendrimers,[13,14] inorganic nanoparticles,[15,16] polymer nanoparticles,[17] and self-assembled nanostructures.[18–20] Among these nanocarriers, self-assembled nanostructures are of particular interest because they can be readily prepared to assume a variety of sizes and shapes with adjustable surface chemistry through solution-state assembly processes. A further attraction is that these supramolecular carriers can dissociate into individual molecules that could be removed through renal clearance once their desired function is accomplished. The limitations of using nanostructured material as drug carriers lie in three aspects. First, their drug carrying capacity is very low, typically below 5% (*w*/*w*). Second, there is an inherent difficulty to control and characterize the amount of drugs loaded in each particle. There will also be a loading variation from particle to particle, and as such the loading capacity only represents the averaged amount of drug loaded in the whole system. Finally, the long term toxicity of these synthetic nano-objects remains unclear.

Our strategy presented here is to devise approaches that enable anticancer drugs to directly assemble into discrete well-defined nanostructures. We first chose two amphiphilic drug molecules, methotrexate (MTX) and folic acid (FA), as proof-of- principle building blocks to illustrate this concept (Scheme 1A). MTX is an antifolate drug used for the treatment of blood, lung, breast, and other kinds of cancer.[21] The mechanism by which MTX exerts its toxicity is through competitive inhibition of dihydrofolate reductase, possessing a one thousand-fold greater binding affinity than folate, which leads to eventual inhibition of DNA and RNA synthesis.[21–23] Folic acid is a biologically active molecule (also known as vitamin M or B_9) that has several important functions in cell sustainability and proliferation, [24] and has been recently reported to be an effective targeting ligand for various cancers.[25] It is known that the pterin (2-aminopteridin-4-ol) moiety could potentially induce a particular arrangement of H-bonding interactions among four FA molecules.[26] Several studies have shown that the resultant Hoogsteen-bonded tetramers of folic acid or its derivatives can stack into chiral columns which further pack into ordered mesophases.[27,26,28–33] Only in a few cases have discrete nanostructures formed by self-assembly of FA or FA derivatives been reported to template the formation of mesoporous silica[34] and to improve the mechanical properties of chitosan hydrogels.[35]

NIH-PA Author Manuscript

NIH-PA Author Manuscript

NIH-PA Author Manuscript

The majority of anticancer drugs are, however, hydrophobic and do not possess the key amphiphilic feature to produce self-assembled discrete nanostructures in aqueous solutions.[36,37] It is therefore necessary to incorporate a small hydrophilic segment onto the drugs of interest. Scheme 1B illustrates the concept of design for a self-assembling drug amphiphile (DA). In this particular case, we conjugated a β-sheet forming peptide onto the hydrophobic drug CPT to impart the necessary amphiphilicity for assembly into discrete nanostructures. This conjugation strategy has been extensively used by a few other groups to create self-assembling peptide amphiphiles,[38–44] peptide nucleic acid amphiphiles,[45] and amphiphiles containing either therapeutic agents[46–49] or π-conjugated aromatic units.[18,50] The peptides sequences used here serve as a structural control unit that play an important role in defining the final morphologies, providing the impetus for one-dimensional elongation through *β*-sheet formation. CPT constitutes not only the bioactive component of the drug amphiphile,[51] but is also the driving force for hydrophobic collapse that helps to initiate self-assembly.[36] Its rigid nature and potential for *π-π* interactions provide further means of influencing the nanostructure morphology formed. Herein, we discuss how solution processing of the nanotube-forming, four CPT-containing drug amphiphile can affect the self-assembly mechanism and provide insight into the stability of such structures.

In both cases of using anticancer drugs as building units, the resulting self-assembled drug nanostructures will 1) have a high drug loading capacity (up to 100% if the nanostructure is made of free drug), 2) allow for a quantitative control of the drug content in each drug carrier since the assembled nanostructures have the identical drug content as the individual molecule, and 3) can minimize the toxicity of using additional synthetic carriers.

Experimental Section

Materials

Folic acid and methotrexate were purchased from Sigma-Aldrich and used as received. Fmoc amino acids, Rink Amide resin and coupling agents (HBTU and HATU) were sourced from AAPPTEC (Louisville, KY) and camptothecin was obtained from Avachem (San Antonio, TX). Borate buffer, consisting of sodium borate decahydrate and sodium hydroxide, was purchased from RICCA Chemical Company. 10×DPBS (Dulbecco's Phosphate Buffered Saline without calcium or magnesium) was purchased from Lonza.

Buffer solutions used in the FA and MTX studies were prepared using the following protocols: Borate buffer (pH 9.5) was used as received; 1×DPBS solution (pH 7.4) was prepared by 10-fold dilution of 10×DPBS with water; 0.1M sodium acetate buffer (pH 5) was prepared by mixing 71.4mL of 0.1M acetic acid and 128.6mL of 0.1M sodium acetate solutions. The pH values of all buffered solutions were measured by a pH meter (Mettler Toledo) using an InLab Micro pH electrode. The solution containing 1 wt% FA was prepared by adding 5.1mg FA to 500*μ*L of each buffer solution and vortexing until clear. The final pH of the solution was subsequently re-adjusted to the initial pH of the original buffer solution by the addition of 1M NaOH or 1M HCl.

Peptide synthesis

The peptide, qCys-Sup35, was synthesized using a combination of automated (Focus XC, AAPPTEC) and manual solid-phase Fmoc peptide synthesis techniques. Branching lysines were introduced through the use of Fmoc-Lys(Fmoc)-OH (Novabiochem, San Diego, CA). The peptide was cleaved from the resin using a mixture of trifluoroacetic acid, triisopropylsilane, water and ethanedithiol (90:5:2.5:2.5) for 2 h, isolating the crude peptide by trituration into cold diethylether. Purification to >95% homogeneity was performed using

NIH-PA Author Manuscript

NIH-PA Author Manuscript

NIH-PA Author Manuscript

reversed-phase HPLC and identifying product fractions by MALDI-TOF mass spectrometry. The desired fractions were then lyophilized to give qCys-Sup35 as a white solid.

Drug amphiphile synthesis

The synthesis of the four CPT-containing drug amphiphile, qCPT-Sup35, was accomplished through the reaction of the peptide qCys-Sup35 with the activated disulphide, CPT-buSS-Pyr (prepared as described previously[36]). Briefly, qCys-Sup35 (15 mg, 6.8 μmol) and CPT-buSS-Pyr (22.8 mg, 40.8 μmol) were dissolved in N_2-purged DMSO (2 ml) and allowed to react for 2 days. The resulting pale yellow solution was then diluted to ~18 ml with 0.1% aq. TFA (adding MeCN as required to solubilise any unreacted CPT-buSS-Pyr). The solution was then purified by reversed-phase HPLC, collecting and lyophilizing the desired product fractions. The resulting powder was dissolved in H_2O and MeCN and aliquotted into cryo-vials, before re-lyophilization. The CPT content was calibrated using a disulphide reduction method and HPLC analysis, indicating that the final yield was 6.8 mg (33%).

Transmission electron microscopy

A drop containing 3–5 μL of liquid samples was loaded onto a carbon-copper TEM grid. Sample solutions were wicked away with a piece of filter paper to result in a thin liquid layer on the grid, and were left to dry for 10 minutes. Next, the dried samples were stained with 5 μL of 2% uranyl acetate aqueous solution. After approximately 10 seconds, excess staining solution was wicked away, and the TEM samples were left to dry for at least 3 h before TEM imaging with a Philips EM 420 TEM equipped with SIS Megaview III CCD digital camera.

Circular dichroism measurements

All circular dichroism (CD) spectra were measured at room temperature using a Jasco J-710 circular dichroism spectrophotometer. In order to obtain consistent CD measurements, samples were diluted 10-fold from 1% to 0.1% FA immediately before each measurement to avoid high tension (HT) values above 800V. A final volume of 200 μL samples were loaded into a 1 mm pathlength cuvette and measurements were obtained from 200 to 450 nm with 0.5 nm data pitch, 200 nm/min scan speed, 2 s response time, and 2 nm band width. The CD spectrum of each sample is the average of 3 measurements with background subtraction and was smoothed by an integrative package in IGOR software.

Results and discussion

Self-assembly of folic acid in methanol-water mixtures

We found that folic acid has a low solubility in pure Milli-Q water but will immediately form a yellowish self-supporting gel upon dissolution in methanol at a concentration of 1% or above (*w*/*v*). TEM imaging reveals dominant filamentous nanostructures (Fig. 1A) with a diameter of 4.2 ± 0.5nm. Inspired by the work of using mixed solvents to control solution-state self-assembly of block copolymers,[52–54] we explored the effect of water-methanol mixtures on the FA assembly. Samples were prepared using two different mixing protocols: a step-wise method and a premixed solvent method.

In the step-wise method, FA was first dissolved in an appropriate amount of pure methanol, followed by the addition of water in a step-wise manner to reach the desired mixing ratio of methanol to water (*v*/*v*). The concentration of FA in all the studied solutions was fixed to be 1% (*w*/*v*). TEM imaging was performed after aging the solutions overnight. As shown in Fig. 1, similar filamentous nanostructures were observed as the dominant morphology in both 80% (Fig. 1B) and 70% (Fig. 1C) methanol solutions, with respective diameters of 3.5 ± 0.5nm and 3.9 ± 0.6 nm. The sample containing 80% methanol also formed a self-

NIH-PA Author Manuscript

NIH-PA Author Manuscript

NIH-PA Author Manuscript

supporting gel, similar to the gel formed in pure methanol. Both could restore the gel state within seconds after vigorous vortexing. The 70% methanol solution on the other hand, while containing a significant amount of nanofibers, presented as a free flowing liquid only. Occasionally, a few lozenge-shaped platelets could be seen by TEM imaging.

These lozenge-shaped platelets became the dominant structures in solutions containing 50% or more water (Figs. 1D–F). On the basis of our TEM observations, most platelets appeared to be single layered, although some multi-layered platelets can also be seen. Frequently, these platelets broke into two halves or even smaller fragments, and thus lost their sharp edges and lozenge shape identity (Fig. 1F). The regular shape and dimension of the observed platelets are strongly reminiscent of those of polymer single crystals,[55] suggesting that the FA molecules are packed in a well-defined order within these platelets.

Circular dichroism (CD) spectroscopy reveals induced supramolecular chirality in both filamentous nanostructures and micron-sized platelets. The CD spectrum of FA in pure water (Fig. 2A, black curve) shows positive bands at 225, 279, and 308 nm, a coupled band centred at 345 nm with two extremes at 328 nm and 362 nm, and a negative peak at 375 nm. All the absorptions above 300 nm are ascribed to the pterin ring which has been shown to have UV–Vis absorptions both at 280nm and around 350 nm in chloroform.[29,33] We speculate that the positive band at 279 nm could be the superposed π-π^* transitions of the pterin ring and the aromatic group adjacent to the glutamic acid. The CD band at 225 nm most likely corresponds to the n–π^* transition of the benzamide group (between the glutamic acid and benzene moieties).

In pure methanol where FA assembles into filamentous nanostructures, the CD spectrum is dramatically different (Fig. 2A, red curve), displaying two negative signals at 225 nm and 273 nm and a weaker, broad positive band around 290 nm. Although FA possesses only one chiral carbon on the glutamic acid, it is not clear to us whether the observed supramolecular chirality is induced solely by glutamic acid packing, or is also affected by the packing of tetramerized pterin rings. It is clear, however, that the differences in CD spectra collected in water and in methanol are a direct reflection of internal chiral packing order. The negative absorption at 225 nm in pure methanol is similar to the characteristic CD absorption of β-sheets, though slightly red shifted. This shift may be due to a combination of the amide being connected to an aromatic moiety and the difference in solvent polarity between water and methanol. Nevertheless, the similarity indicates that glutamic acid may pack in a similar fashion to that found in β-sheet assemblies, helping to propagate the one-dimensional elongation. It is highly possible that the adjacent aromatic group, under the direct influence of this chiral packing, is induced to give rise to a similar negative absorption around 270 nm. With increasing water content in the step-wise method, both negative absorptions became positive in amplitude and gradually intensified, and at the same time the positive absorptions linked to the pterin rings became stronger. The observed change in sign of absorption suggests a different packing order between the filaments and the platelets. Also, the increasing intensity of the CD band around 280 nm as the methanol percentage decreases implies that more stable chiral aggregates are formed in low methanol content mixtures.

We found the self-assembly of FA, particularly the formation of FA nanofibers, in methanol-water mixtures to be pathway-dependant. In the pre-mixed method, FA was directly dissolved in previously prepared water-methanol mixtures (80%, 70%, 50% and 25% *v*/*v* methanol). All solutions that were studied exhibited micro-lozenge formation only, with no evidence of any filamentous nanostructures (Figs. 3A–D). CD analysis of these solutions indicated these structures possessed the same secondary structure and packing modes as those formed by the step-wise addition method (Fig. 2B). These experiments

NIH-PA Author Manuscript

NIH-PA Author Manuscript

NIH-PA Author Manuscript

suggest that water plays a significant role in the formation of the platelet structures, while methanol seems to favour the filamentous nanostructures.

The TEM studies and CD measurements collectively suggest that the observed nanofibers in pure methanol are one-dimensional stacks of FA tetramers. It has been shown by a number of laboratories that FA and its derivatives are capable of forming Hoogsteen-bonded tetrads through self-recognition of the pterin rings that contain both H-bond donors and acceptors.[28–31] The resulting disklike tetramers can form one-dimensional nanostructures that further stack into hexagonal mesophases.[28–31] In the case reported here, the diameters of the nanofibers are in the range of 3.5 to 4 nm, which are in good agreement with the expected width of the disklike tetramers. Other evidence comes from the studies on the self-assembly of MTX. Our results showed that MTX could not form any well-defined nanostructures in all the studied conditions. In the case of MTX, the H-bond donor C=O in the pterin ring is replaced with the $-NH_2$ group. This replacement appears to prevent it from forming the tetrameric disks that can aggregate into defined nanostructures. This is consistent with studies on the interaction of FA and MTX with the dihydrofolate reductase enzyme, which showed the two molecules binding with strikingly different orientations as a result of their differing H-bond donor/acceptor arrangements.[56,22] It can therefore be concluded that, the formation of the tetrameric structure represents the first step toward the formation of all the observed morphologies.

The driving forces for one-dimensional stacking of tetrads could possibly stem from combined contributions of both the associative interactions between the tetramerized pterin rings (π–π stacking) and the hydrogen bonding between the glutamic acid segments. In pure methanol, where only discrete nanofibers were observed, this stacking seems to be rather loose as the CD spectrum (Fig. 2A) reveals only the absorption bands linked to the glutamic acid and the adjacent aromatic ring, with the pterin moiety showing only weakly induced supramolecular chirality.

Addition of water into methanol solutions containing FA nanofibers leads to the transition from nanofibers to lozenge platelets. The stacking of the FA columns into lozenge platelets is likely driven by inter-fiber interactions of the *C*-terminal and side-chain carboxylic acid groups. At the same time, the significant increase in the intensity of the pterin-associated CD signals also suggests changes in internal packing between the FA tetrads. It is therefore reasonable to assume that the supramolecular chirality of the pterin rings is linked to the crystalline packing among the FA columns. It is also possible that the increasing water content may affect the packing between the tetramerized pterin rings, leading to more compacted and ordered packing among them.

Self-assembly of folic acid at different pH

The proposed model in Figure 4 leads us to assume that at relatively higher pH values, at which carboxylic acid groups became highly deprotonated, the electrostatic repulsions will likely dissociate the lozenge platelets into individual nanostructures. We therefore carried out a series of experiments using three different buffers: sodium acetate buffer (buffer zone: ~5), phosphate buffered saline (buffer zone: ~7.5), and borate buffer (buffer zone: ~9.5). FA was directly dissolved in the buffered solutions and their pH was carefully monitored and readjusted to be within their respective buffer zones if necessary. FA was found to have a very low solubility in acetate buffer. Fig. 5A reveals that fragmented platelets were the dominant nanostructure formed under these conditions. It should be noted that a 1 wt% solution of FA in pure water is also around pH 5, and so it would be expected that a buffered solution at this pH would give similar structures. At pH 7.4 (1× DPBS buffer) FA was observed to self-assemble into 1D nanostructures with an average diameter of 4.1 ± 0.4 nm (Fig. 5B). These nanofibers are remarkably similar to those formed in pure methanol. At pH

NIH-PA Author Manuscript

NIH-PA Author Manuscript

NIH-PA Author Manuscript

9.5 (borate buffer), much shorter nano fibers were observed with an average diameter of 4.0 ± 0.4 nm. It is very likely that electrostatic repulsions among glutamic acid segments as a result of almost complete deprotonation at this pH are responsible for the short length of nanofibers.

CD measurements were then obtained to probe the internal structure of the FA assemblies formed at three buffered solutions (Fig. 5D). Nanofiber-dominated samples in both buffered solutions (1×DPBS and borate) consistently showed a characteristic negative peak around 220–225 nm, indicative of the $n \rightarrow \pi^*$ transition of the amide group. However, compared to the CD spectra collected from pure methanol, the CD signals of FA in 1×DPBS and borate buffers did not exhibit the negative peak at 273 nm that was observed for the pure methanol samples, instead showing a very weak positive band. The reason for this may lie in the nature of the solvent system used. Since methanol is less polar than water, the spacing between the stacked tetrads may be increased as there is less need to shield the more hydrophobic pterin rings from the bulk solvent.[57] This would lessen interactions between adjacent layers, and as such the induced chirality would be determined to a great extent by the chiral packing between the glutamic acid segments, only giving rise to the negative signal observed at 273 nm. The aqueous buffers 1×DPBS and borate, on the other hand, are polar that may cause the layers to stack more tightly, thereby contributing greatly to the induced supramolecular chirality and shifting the signal toward a positive amplitude.

Similar to the CD spectra observed in water and aqueous methanol mixtures, 1 wt% solutions of FA in water and sodium acetate exhibited almost identical intense pterin ring absorptions over the 270–400 nm range. In addition, the 225 nm CD signal due to the amide group had a positive amplitude for the water and sodium acetate buffer solutions, as previously observed for the platelet structures. These observations show a clear correlation with the morphology that is adopted and can be used as a predictor for the structure formed. Filamentous structures correspond to a negative peak in the 220–225 nm region, whereas the platelet structure is indicated by a positive peak in the 220–225 nm region and multiple strong pterin ring absorptions.

Comparing the results from the buffered solutions, it is clear that the stacking of the filamentous structures to form the micro-lozenges is dependent upon shielding of the carboxylic acid groups of the glutamate residue. In pure water, methanolic water and sodium acetate buffer, there is partial shielding of the negative charges that allows the filaments to pack together and ultimately yield the platelet structure. It is likely that water will help to bridge the filaments through hydrogen bonding interactions. In 1×DPBS and borate, however, there is insufficient shielding and the negative charges introduce strong repulsive forces between the individual filaments that prevents association with one another. Accordingly, only one-dimensional structures are observed in these conditions. The case of methanol is likely different as this less polar solvent will favour the more protonated state of the carboxylic acids due to its lower ability to solvate charges. The lack of micro-lozenge structure is therefore a consequence of methanol being unable to act as a hydrogen bonding bridge between the carboxylic acids.

Nanotubes formed by self-assembly of CPT drug amphiphiles

The conjugation of a peptide segment with overall hydrophilicity onto the hydrophobic drug camptothecin creates amphiphilic molecules that could potentially self-assemble into discrete nanostructures in an aqueous environment.[36,37] The resulting supramolecular nanostructures, regardless of the size, shape, or morphologies, would contain the same drug loading as the individual molecule. Here we discuss our efforts to probe the self-assembly pathway of drug amphiphiles (DAs) that were found to form a nanotube morphology. These DAs were synthesized by attaching four CPT molecules to a β-sheet-forming peptide. In this

NIH-PA Author Manuscript

NIH-PA Author Manuscript

NIH-PA Author Manuscript

study, we used peptide sequences derived from the Tau protein[58] and the Sup35 yeast prion[59] that are both capable of forming parallel β-sheet assemblies. After conjugation with four CPT units, the drug loadings are 38% (*w*/*w*) for qCPT-Tau and 36% (*w*/*w*) for qCPT-sup35.

The self-assembly of the two synthesized drug amphiphiles was initially probed by dissolving the respective conjugates into water (100 μM) and using TEM to determine the assembly morphology. It can be seen from Fig. 6 that both qCPT-Tau (Fig. 6A) and qCPT-Sup35 (Fig. 6B) formed nanotubes with outer diameters of 9.5 ± 1.0 nm and 9.9 ± 1.1 nm, respectively. The tubular morphology is inferred by the dark centre line throughout the observed filamentous morphologies due to the preferential deposition of the staining agent uranyl acetate onto the collapsed cores. These results also suggest that the replacement of the Tau β-sheet-forming peptide with the Sup35 β-sheet-forming peptide has little or no effect on the nanostructure morphology. The only notable difference was the longer contour length of the Sup35-based nanotubes, which may be due to the greater solubility of this conjugate compared with the Tau-based conjugate. CD spectroscopy further reveals that the two assembled conjugates possess similar packing arrangements (Fig. 6C), with both displaying excitonic coupling that arises from electronic interactions between neighbouring CPT units. Strong β-sheet signals can also be seen for both conjugates, albeit red-shifted to around 224 nm from the typical value of 216 nm. We noted that the organic solvent DMSO can disrupt the nanotube structures, as the CD spectrum of qCPT-Tau in DMSO only displays a weak negative signal, most likely due to the drug's own chirality.

We found that assembly into nanotubes is also a path-dependent process. In these experiments, we first used hexafluoroisopropanol (HFIP) to break any pre-existing aggregates formed by the conjugates during purification and lyophilisation. HFIP is a fluorous solvent commonly used for the solubilisation of amyloid-forming peptides. We chose HFIP over DMSO as its volatility allows for easy removal. After removal of HFIP, the qCPT-Sup35 residue was reconstituted in water to reach a final concentration of 100 μM, however a turbid solution was formed that contained visible aggregates. TEM imaging after overnight aging did not show any dominant well-defined structures except for the occasional observation of several short fibers or tubes (Fig. 7B). We speculate that the thin films formed upon drying of the HFIP solution were too insoluble in water, possibly due to strong interactions among the CPT segments that prevented any structural rearrangement on our experimental timescale. However, when a mixture of water and acetonitrile (50/50) was used to reconstitute the HFIP-treated sample, a clear solution was formed immediately. Interestingly, TEM imaging (Fig. 7C) shows nanofibers to be the dominant structure rather than the tubular morphology formed without HFIP-treatment (Fig. 7A). The diameter of these nanofibers is 5.8 ± 0.7 nm, a value much smaller than the outer diameter of the nanotubes (9.9 ± 1.1 nm), indicative of a possible core-shell micellar structure.

CD spectroscopy of this solution (Fig. 7D) shows that the level of electronic interaction between CPT units is strongly diminished in comparison to that of the nanotube morphology, with no bisignate peaks observed in the CPT absorption regions. The continued presence of the peak around 389 nm does, however, suggest that there still exist some CPT–CPT interactions, perhaps due to interactions between CPT molecules of the same conjugate. It is also evident that the CD spectrum of the nanofiber solution exhibits a more typical β-sheet signal at 216 nm, rather than the red-shifted and more intense signal observed for the nanotube structure. These experiments reveal that even for small molecule amphiphiles, the resulting self-assembled structure could still be kinetically trapped due to the involvement of molecular interactions such as hydrogen bonds or π-π interactions that provide strong stabilization when present in a large number.

NIH-PA Author Manuscript

NIH-PA Author Manuscript

NIH-PA Author Manuscript

Conclusion

In this discussion, we reported our work on the self-assembly of small molecule drugs in dilute solutions. First of all, we demonstrated the possibility of using drug molecules as molecular building blocks to create discrete supramolecular nanostructures. We showed that the free folic acid can assemble into both nanofibers and micro-sized lozenges depending on the solvent conditions and mixing procedures. In the case of hydrophobic anticancer drugs, conjugation to a peptide segment with overall hydrophilicity presents an effective strategy to create self-assembling drug amphiphiles that have the ability to assemble into discrete nanostructures. Second, we demonstrated the tunability of the resulting supramolecular nanostructures, for example, the morphological transition from nanofibers to lozenges for folic acid, and also the transition from nanotubes to nanofibers in the case of CPT drug amphiphiles. Third, we demonstrated the complexity of assembling small molecule drugs. Unlike traditional low-molecular-weight surfactants which are known to assemble into dynamic, thermodynamically stable micellar structures, small molecule drugs often posses the ability to form strong intermolecular interactions such as hydrogen bonding, or π-π interactions. These strong interactions are critical for the drug's biological functions. The presence of these interactions is twofold: on one hand, it allows for the formation of stable, far-from-equilibrium nanostructures in dilute solutions. Stability is often a very important consideration in the design of supramolecular drug carriers. On the other hand, it results in difficulties in understanding the path-dependent assembly behaviours.

Acknowledgments

We thank National Science Foundation (DMR 1255281) for support of the project, and NIH for funding A.C. (T-32CA130840) and Y.L. (R25CA153952). We thank the JHU Integrated Imaging Center (IIC) for the use of the TEM facility, and the JHU Department of Chemistry Mass Spectrometry facility for MALDI-ToF (NSF CHE-0840463) and ESI analysis. We also thank Prof. Kalina Hristova (MSE, JHU) for the use of CD spectrometer.

References

1. Langer R. Drug delivery and targeting. Nature. 1998; 392:5–10. [PubMed: 9579855]
2. Duncan R. The dawning era of polymer therapeutics. Nature Reviews Drug Discovery. 2003; 2:347–360.
3. Duncan R. Polymer conjugates as anticancer nanomedicines. Nature Reviews Cancer. 2006; 6:688–701.
4. Haag R, Kratz F. Polymer therapeutics: Concepts and applications. Angewandte Chemie-International Edition. 2006; 45:1198–1215.
5. Kataoka K, Harada A, Nagasaki Y. Block copolymer micelles for drug delivery: design, characterization and biological significance. Advanced Drug Delivery Reviews. 2001; 47:113–131. [PubMed: 11251249]
6. Li SD, Huang L. Pharmacokinetics and biodistribution of nanoparticles. Molecular Pharmaceutics. 2008; 5:496–504. [PubMed: 18611037]
7. Peer D, Karp JM, Hong S, FaroKhzad OC, Margalit R, Langer R. Nanocarriers as an emerging platform for cancer therapy. Nature Nanotechnology. 2007; 2:751–760.
8. Schroeder A, Heller DA, Winslow MM, Dahlman JE, Pratt GW, Langer R, Jacks T, Anderson DG. Treating metastatic cancer with nanotechnology. Nature Reviews Cancer. 2012; 12:39–50.
9. Torchilin VP. Multifunctional nanocarriers. Advanced Drug Delivery Reviews. 2006; 58:1532–1555. [PubMed: 17092599]
10. Nel AE, Madler L, Velegol D, Xia T, Hoek EMV, Somasundaran P, Klaessig F, Castranova V, Thompson M. Understanding biophysicochemical interactions at the nano-bio interface. Nature Materials. 2009; 8:543–557.
11. Torchilin VP. Recent advances with liposomes as pharmaceutical carriers. Nature Reviews Drug Discovery. 2005; 4:145–160.

NIH-PA Author Manuscript NIH-PA Author Manuscript NIH-PA Author Manuscript

12. Discher DE, Eisenberg A. Polymer vesicles. Science. 2002; 297:967–973. [PubMed: 12169723]
13. Lee CC, MacKay JA, Frechet JMJ, Szoka FC. Designing dendrimers for biological applications. Nature Biotechnology. 2005; 23:1517–1526.
14. Patri AK, Kukowska-Latallo JF, Baker JR. Targeted drug delivery with dendrimers: Comparison of the release kinetics of covalently conjugated drug and non-covalent drug inclusion complex. Advanced Drug Delivery Reviews. 2005; 57:2203–2214. [PubMed: 16290254]
15. Ghosh P, Han G, De M, Kim CK, Rotello VM. Gold nanoparticles in delivery applications. Advanced Drug Delivery Reviews. 2008; 60:1307–1315. [PubMed: 18555555]
16. Paciotti GF, Myer L, Weinreich D, Goia D, Pavel N, McLaughlin RE, Tamarkin L. Colloidal gold: A novel nanoparticle vector for tumor directed drug delivery. Drug Delivery. 2004; 11:169–183. [PubMed: 15204636]
17. Euliss LE, DuPont JA, Gratton S, DeSimone JM. Imparting size, shape, and composition control of materials for nanomedicine. Chemical Society Reviews. 2006; 35:1095–1104. [PubMed: 17057838]
18. Aida T, Meijer EW, Stupp SI. Functional Supramolecular Polymers. Science. 2012; 335:813–817. [PubMed: 22344437]
19. Cabral H, Nishiyama N, Kataoka K. Supramolecular Nanodevices: From Design Validation to Theranostic Nanomedicine. Accounts of Chemical Research. 2011; 44:999–1008. [PubMed: 21755933]
20. Geng Y, Dalhaimer P, Cai SS, Tsai R, Tewari M, Minko T, Discher DE. Shape effects of filaments versus spherical particles in flow and drug delivery. Nature Nanotechnology. 2007; 2:249–255.
21. Jolivet J, Cowan KH, Curt GA, Clendeninn NJ, Chabner BA. The Pharmacology and Clinical Use of Methotrexate. New England Journal of Medicine. 1983; 309:1094–1104. [PubMed: 6353235]
22. Ozaki Y, King RW, Carey PR. Methotrexate and folate binding to dihydrofolate-reductase - separate characterization of the pteridine and para-aminobenzoyl binding-sites by resonance raman-spectroscopy. Biochemistry. 1981; 20:3219–3225. [PubMed: 7018571]
23. Szakacs Z, Noszai B. Determination of dissociation constants of folic acid, methotrexate, and other photolabile pteridines by pressure-assisted capillary electrophoresis. Electrophoresis. 2006; 27:3399–3409. [PubMed: 16944455]
24. Lucock M. Folic acid: Nutritional biochemistry, molecular biology, and role in disease processes. Molecular Genetics and Metabolism. 2000; 71:121–138. [PubMed: 11001804]
25. Low PS, Henne WA, Doorneweerd DD. Discovery and development of folic-acid-based receptor targeting for Imaging and therapy of cancer and inflammatory diseases. Accounts of Chemical Research. 2008; 41:120–129. [PubMed: 17655275]
26. Ciuchi F, Dinicola G, Franz H, Gottarelli G, Mariani P, Bossi MGP, Spada GP. Self-Recognition and Self-Assembly of Folic-Acid Salts - Columnar Liquid-Crystalline Polymorphism and the Column Growth-Process. Journal of the American Chemical Society. 1994; 116:7064–7071.
27. Bonazzi S, Demorais MM, Gottarelli G, Mariani P, Spada GP. Self-Assembly and Liquid-Crystal Formation of Folic-Acid Salts. Angewandte Chemie-International Edition in English. 1993; 32:248–250.
28. Gottarelli G, Mezzina E, Spada GP, Carsughi F, DiNicola G, Mariani P, Sabatucci A, Bonazzi S. The self-recognition and self-assembly of folic acid salts in isotropic water solution. Helvetica Chimica Acta. 1996; 79:220–234.
29. Kamikawa Y, Nishii M, Kato T. Self-assembly of folic acid derivatives: Induction of supramolecular chirality by hierarchical chiral structures. Chemistry-a European Journal. 2004; 10:5942–5951.
30. Kamikawa Y, Nishii M, Kato T. Supramolecular chiral cubic phases formed by folic acid derivatives. Molecular Crystals and Liquid Crystals. 2005; 435:755–765.
31. Kanie K, Nishii M, Yasuda T, Taki T, Ujiie S, Kato T. Self-assembly of thermotropic liquid-crystalline folic acid derivatives: hydrogen-bonded complexes forming layers and columns. Journal of Materials Chemistry. 2001; 11:2875–2886.
32. Kato T. Self-assembly of phase-segregated liquid crystal structures. Science. 2002; 295:2414–2418. [PubMed: 11923528]

NIH-PA Author Manuscript

NIH-PA Author Manuscript

NIH-PA Author Manuscript

33. Kato T, Matsuoka T, Nishii M, Kamikawa Y, Kanie K, Nishimura T, Yashima E, Ujiie S. Supramolecular chirality of thermotropic liquid-crystalline folic acid derivatives. Angewandte Chemie-International Edition. 2004; 43:1969–1972.
34. Atluri R, Hedin N, Garcia-Bennett AE. Nonsurfactant Supramolecular Synthesis of Ordered Mesoporous Silica. Journal of the American Chemical Society. 2009; 131:3189. [PubMed: 19220057]
35. Chakraborty P, Roy B, Bairi P, Nandi AK. Improved mechanical and photophysical properties of chitosan incorporated folic acid gel possessing the characteristics of dye and metal ion absorption. Journal of Materials Chemistry. 2012; 22:20291–20298.
36. Cheetham AG, Zhang PC, Lin YA, Lock LL, Cui HG. Supramolecular Nanostructures Formed by Anticancer Drug Assembly. Journal of the American Chemical Society. 2013; 135:2907–2910. [PubMed: 23379791]
37. Lin R, Cheetham AG, Zhang PC, Lin YA, Cui HG. Supramolecular filaments containing a fixed 41% paclitaxel loading. Chemical Communications. 2013; 49:4968–4970. [PubMed: 23612448]
38. Cui HG, Pashuck ET, Velichko YS, Weigand SJ, Cheetham AG, Newcomb CJ, Stupp SI. Spontaneous and X-ray-Triggered Crystallization at Long Range in Self-Assembling Filament Networks. Science. 2010; 327:555–559. [PubMed: 20019248]
39. Cui HG, Webber MJ, Stupp SI. Self-Assembly of Peptide Amphiphiles: From Molecules to Nanostructures to Biomaterials. Biopolymers. 2010; 94:1–18. [PubMed: 20091874]
40. Hamley IW, Krysmann MJ, Castelletto V, Noirez L. Multiple Lyotropic Polymorphism of a Poly(ethylene glycol)-Peptide Conjugate in Aqueous Solution. Advanced Materials. 2008; 20:4394–4397.
41. Hartgerink JD, Beniash E, Stupp SI. Self-assembly and mineralization of peptide-amphiphile nanofibers. Science. 2001; 294:1684–1688. [PubMed: 11721046]
42. Lowik D, van Hest JCM. Peptide based amphiphiles. Chemical Society Reviews. 2004; 33:234–245. [PubMed: 15103405]
43. Trent A, Marullo R, Lin B, Black M, Tirrell M. Structural properties of soluble peptide amphiphile micelles. Soft Matter. 2011; 7:9572–9582.
44. Yu YC, Berndt P, Tirrell M, Fields GB. Self-assembling amphiphiles for construction of protein molecular architecture. Journal of the American Chemical Society. 1996; 118:12515–12520.
45. Vernille JP, Kovell LC, Schneider JW. Peptide nucleic acid (PNA) amphiphiles: Synthesis, self-assembly, and duplex stability. Bioconjugate Chemistry. 2004; 15:1314–1321. [PubMed: 15546198]
46. Gao Y, Kuang Y, Guo ZF, Guo ZH, Krauss IJ, Xu B. Enzyme-Instructed Molecular Self-assembly Confers Nanofibers and a Supramolecular Hydrogel of Taxol Derivative. Journal of the American Chemical Society. 2009; 131:13576. [PubMed: 19731909]
47. Gao Y, Zhao F, Wang QG, Zhang Y, Xu B. Small peptide nanofibers as the matrices of molecular hydrogels for mimicking enzymes and enhancing the activity of enzymes. Chemical Society Reviews. 2010; 39:3425–3433. [PubMed: 20623068]
48. Li JY, Kuang Y, Gao Y, Du XW, Shi JF, Xu B. D-Amino Acids Boost the Selectivity and Confer Supramolecular Hydrogels of a Nonsteroidal Anti-Inflammatory Drug (NSAID). Journal of the American Chemical Society. 2013; 135:542–545. [PubMed: 23136972]
49. Li XM, Kuang Y, Xu B. “Molecular trinity” for soft nanomaterials: integrating nucleobases, amino acids, and glycosides to construct multifunctional hydrogelators. Soft Matter. 2012; 8:2801–2806.
50. Peeters E, Delmotte A, Janssen RAJ, Meijer EW. Chiroptical properties of poly{2,5-bis (S)-2-methylbutoxy -1,4-phenylene vinylene}. Advanced Materials. 1997; 9:493.
51. Pommier Y. Topoisomerase I inhibitors: camptothecins and beyond. Nature Reviews Cancer. 2006; 6:789–802.
52. Cui HG, Chen ZY, Wooley KL, Pochan DJ. Controlling micellar structure of amphiphilic charged triblock copolymers in dilute solution via coassembly with organic counterions of different spacer lengths. Macromolecules. 2006; 39:6599–6607.
53. Cui HG, Chen ZY, Zhong S, Wooley KL, Pochan DJ. Block copolymer assembly via kinetic control. Science. 2007; 317:647–650. [PubMed: 17673657]

NIH-PA Author Manuscript

NIH-PA Author Manuscript

NIH-PA Author Manuscript

54. Zhu JH, Zhang SY, Zhang FW, Wooley KL, Pochan DJ. Hierarchical Assembly of Complex Block Copolymer Nanoparticles into Multicompartment Superstructures through Tunable Interparticle Associations. Advanced Functional Materials. 2013; 23:1767–1773.

55. Reneker DH, Geil PH. Morphology of Polymer Single Crystals. Journal of Applied Physics. 1960; 31:1916–1925.

56. Goodsell DS. The molecular perspective: Methotrexate. Stem Cells. 1999; 17:314–315. [PubMed: 10527466]

57. Cubberley MS, Iverson BL. H-1 NMR investigation of solvent effects in aromatic stacking interactions. Journal of the American Chemical Society. 2001; 123:7560–7563. [PubMed: 11480976]

58. Goux WJ, Kopplin L, Nguyen AD, Leak K, Rutkofsky M, Shanmuganandam VD, Sharma D, Inouye H, Kirschner DA. The formation of straight and twisted filaments from short tau peptides. Journal of Biological Chemistry. 2004; 279:26868–26875. [PubMed: 15100221]

59. Nelson R, Sawaya MR, Balbirnie M, Madsen AO, Riekel C, Grothe R, Eisenberg D. Structure of the cross-beta spine of amyloid-like fibrils. Nature. 2005; 435:773–778. [PubMed: 15944695]

NIH-PA Author Manuscript

NIH-PA Author Manuscript

NIH-PA Author Manuscript

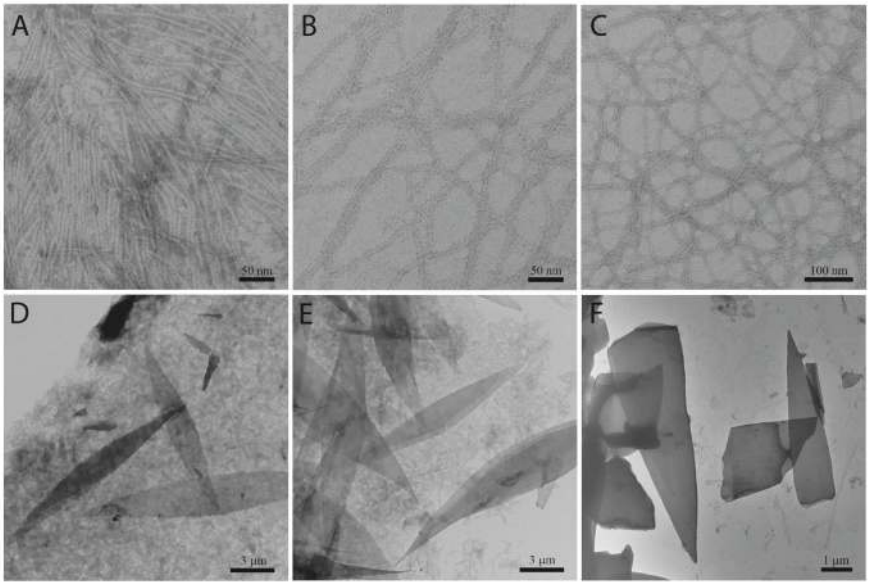

Figure 1.

TEM images of self-assembled filamentous nanostructures and micron-sized platelets formed by 1 wt% folic acid in mixtures of methanol and water. The samples were prepared through a stepwise mixing method through which folic acid was first dissolved in methanol with subsequent addition of water to reach the desired mixing ratio. Filamentous nanostructures were observed as the dominant morphology in solution samples containing 100% (A), 80% (B), and 70% (C) methanol, with a diameter of 4.2±0.5 nm, 3.5±0.5 nm and 3.9±0.6 nm respectively. Lozenge-shaped platelets of micron size were dominant in solutions containing 50% (D), 25% (E) and 0% (F) methanol.

NIH-PA Author Manuscript

NIH-PA Author Manuscript

NIH-PA Author Manuscript

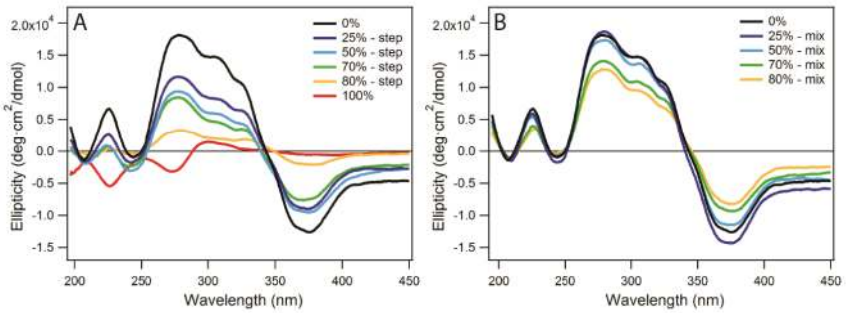

Figure 2.

Circular dichroism spectra of 1wt% folic acid solutions in methanol-water mixtures of varying compositions, prepared by two different methods: step-wise addition of water to a methanolic solution of folic acid (**A**) and dissolution of folic acid in pre-mixed methanol-water mixtures (**B**).

NIH-PA Author Manuscript

NIH-PA Author Manuscript

NIH-PA Author Manuscript

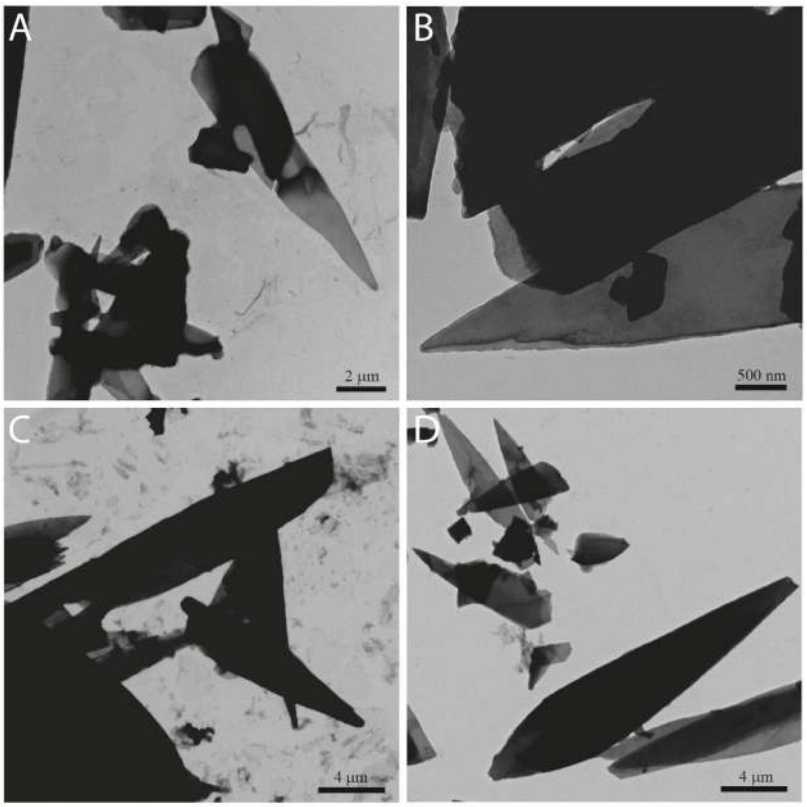

Figure 3.
TEM images of micron-sized, lozenge-shaped platelets at mixed solvents containing 80% (**A**), 70% (**B**), 50% (**C**) and 25% (**D**) methanol. The samples were prepared by directly dissolving folic acid into the mixed solvents with predetermined ratio to reach a final concentration of 1%.

NIH-PA Author Manuscript

NIH-PA Author Manuscript

NIH-PA Author Manuscript

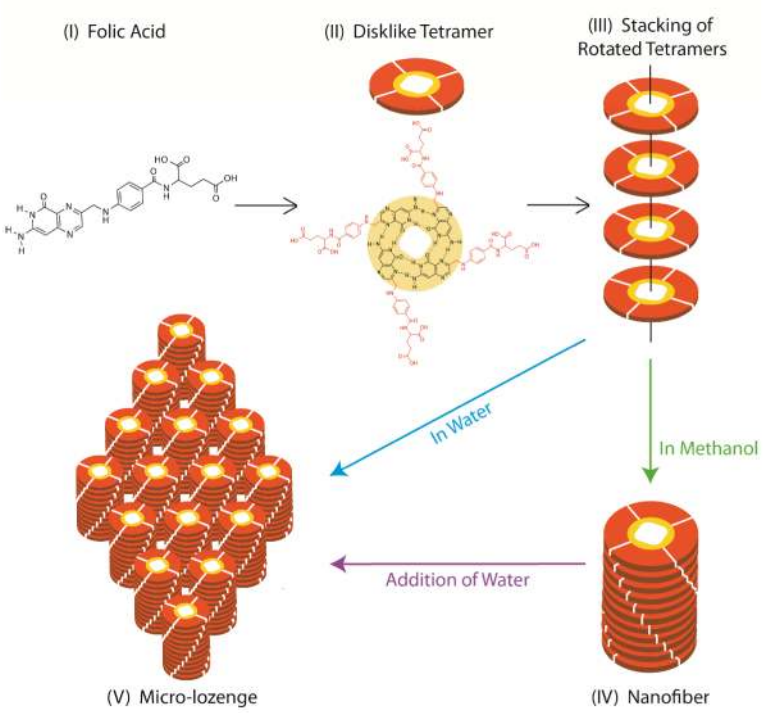

Figure 4.

Proposed self-assembly pathways of folic acid into nanofibers and micro-lozenges. The pterin ring of folic acid (I) interacts with two adjacent folic acid molecules through Hoogsteen H-bond to form disklike tetramers (II). These tetramers stack up in a rotated manner (III) to form a nanofiber (IV) in methanol. These stacked columns can further associate to give lozenge-shaped platelets in water (V). Addition of water into nanofiber-containing methanol solution leads to a morphological transition into platelets.

NIH-PA Author Manuscript
NIH-PA Author Manuscript
NIH-PA Author Manuscript

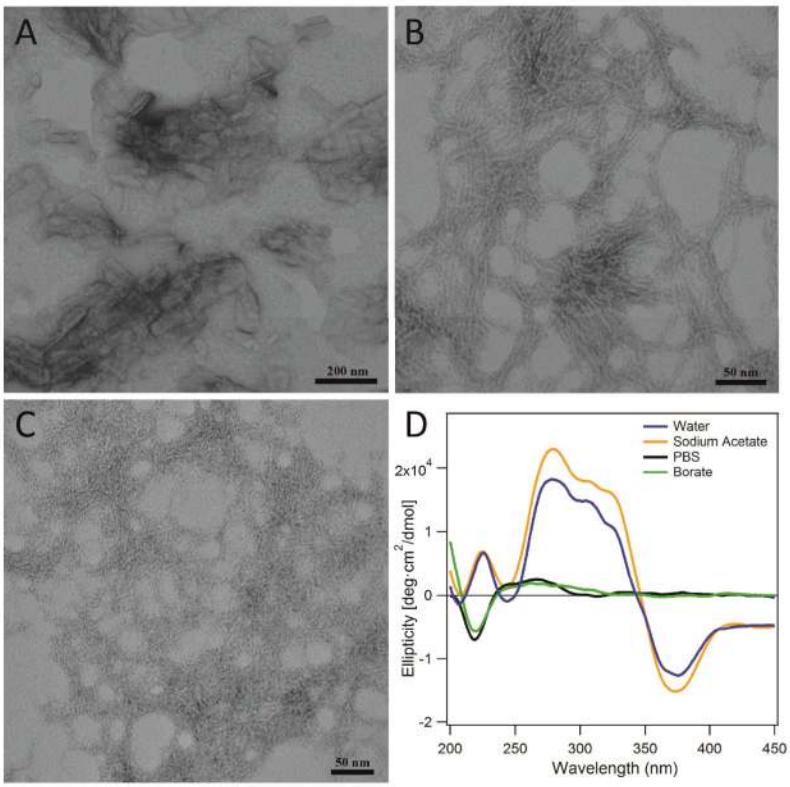

Figure 5.

TEM images of folic acid formed at three different buffers (**A**–**C**) and their corresponding CD spectra (**D**). (**A**) Sodium acetate buffer (pH 5), (**B**) 1×DPBS (~pH 7.4), and (**C**) borate buffer (~pH 9.5).

NIH-PA Author Manuscript

NIH-PA Author Manuscript

NIH-PA Author Manuscript

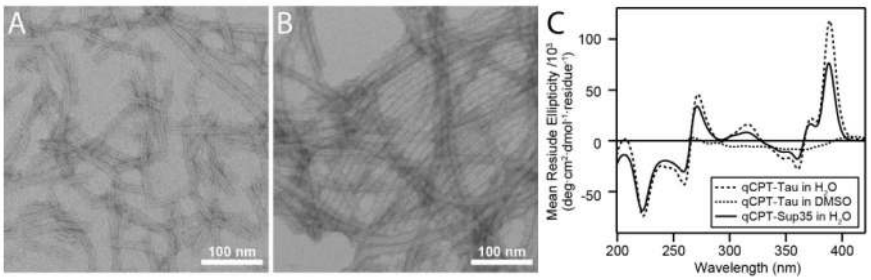

Figure 6.

Representative TEM micrographs of nanotubes formed by qCPT-Tau (**A**) and qCPT-Sup35 (B) in water at 100 μM. TEM samples were negatively stained with 2% uranyl acetate. (**C**) Circular dichroism spectra of qCPT-Tau in water (1 μM) and DMSO (500 nM), and qCPT-Sup35 (50 μM) in water.

NIH-PA Author Manuscript

NIH-PA Author Manuscript

NIH-PA Author Manuscript

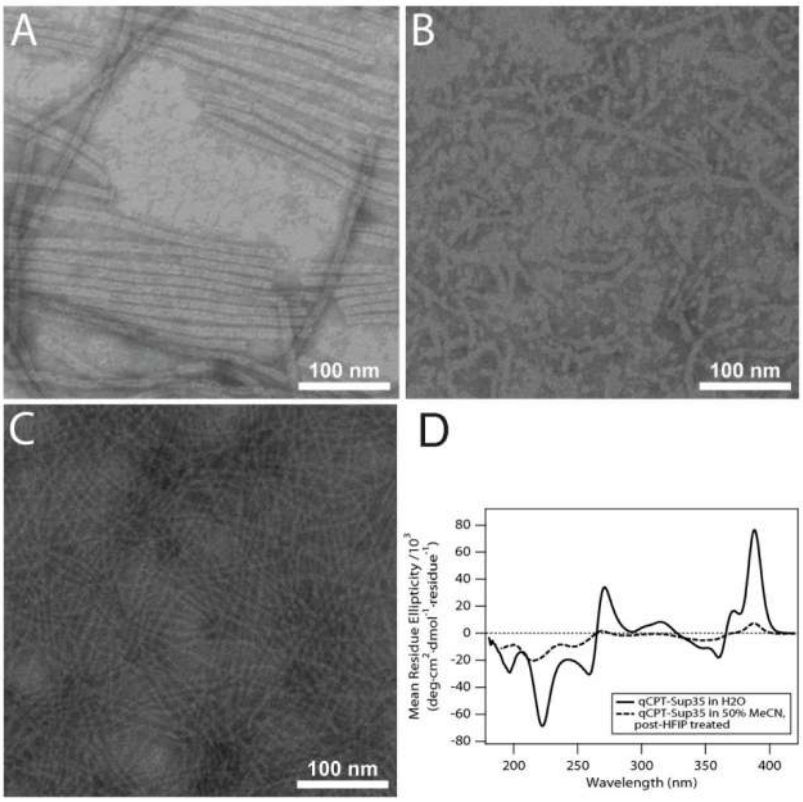

Figure 7.

TEM micrographs of the assembled structures formed by qCPT-Sup35 via different preparative pathways. Nanotubes of qCPT-Sup35 were observed after dissolution in water at 100 μM after peptide purification (**A**). Only very few short nanofibers were observed upon reconstitution of qCPT-Sup35 in water at 100 μM after initial lyophilization from HFIP (**B**). Core-shell nanofibers were observed as the dominant structures when qCPT-Sup35 was reconstituted at 50 μM in 50% aqueous MeCN after initial lyophilization from HFIP (**C**). All TEM samples were negatively stained by 2% uranyl acetate. (**D**) CD spectra of qCPT-Sup35 in H_2O (solid line, 50μM), where nanotubes are the dominant self-assembly morphology, and qCPT-Sup35 in 50% aqueous MeCN after lyophilization from HFIP (dashed line, 50 μM). The latter process of solution preparation favors the formation of single filaments rather than nanotubes.

NIH-PA Author Manuscript

NIH-PA Author Manuscript

NIH-PA Author Manuscript

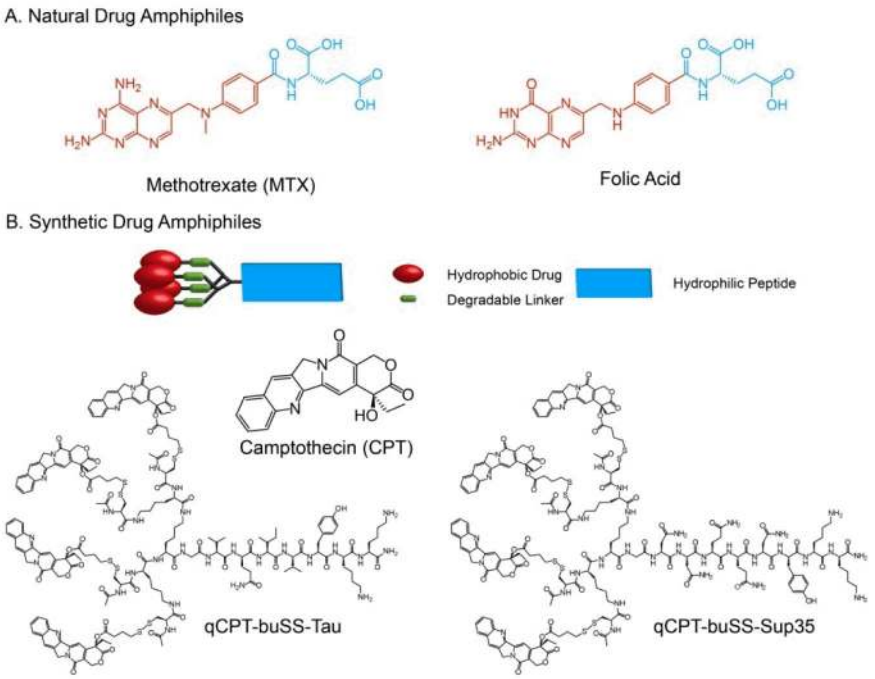

Scheme 1.

Chemical structures of natural and synthetic drug amphiphiles used in this study.**(A**) Both methotrexate and folic acid contain a glutamic acid residue (marked in blue) and can be regarded as amphiphilic molecules when deprotonated at a higher pH. (**B**) The creation of camptothecin (CPT) drug amphiphiles by conjugating four CPT molecules to one *β*-sheet forming peptide via a biodegradable linker. Two *β*-sheet forming sequences (VQIVYK and NNQQNY) were used to create two drug amphiphiles: qCPT-buSS-Tau and qCPT-buSS-Sup35. The linker used to bridge the drug and the peptide is responsive to glutathione, a reducing agent within cells.